

Supporting Information for
“The removals of disulfide bonds in amylin oligomers lead to the conformational change of the 'native' amylin oligomers”

Vered Wineman-Fisher,^{1,2} Lucia Tudorachi,³ Einav Nissim^{1,2} and Yifat Miller^{1,2}

¹Department of Chemistry, Ben-Gurion University of the Negev, P.O. Box 653, Be'er Sheva 84105, Israel

²Ilse Katz Institute for Nanoscale Science and Technology, Ben-Gurion University of the Negev, Beér-Sheva 84105, Israel

³Al. I. Cuza University of Iasi, 11 Carol I, Iasi-700506, Romania

Corresponding Author:

Yifat Miller

E-mail: ymiller@bgu.ac.il

Fax: +972-86428709

Tel: +972-86428705

Material and Methods

1. Constructed models

We applied models M1, M2, M5 and M6 from our previous study on amylin oligomers¹ and annotated here as models M1, M2, M3 and M4, respectively. In each model we removed the disulfide bond in the amylin oligomers and annotated models M1, M2, M3 and M4 as models D1, D2, D3 and D4, respectively. We further constructed models in which we deleted in models M1-M4 the N-terminal residues Lys1-Cys7 by applying the Accelrys Discovery Studio software package (<http://accelrys.com/products/discovery-studio/>), we then extended the sequence of amylin(8-37) of each monomer within the oligomer to Lys1-Cys7, forming β -strands. These models were annotated as E1, E2, E3 and E4. In other words, the initial models E1-E4 the Lys1-Ala18 illustrates β -strand.

2. Molecular dynamics (MD) simulations protocol

We constructed amylin fibril-like structural models by using the Accelrys Discovery Studio software package (<http://accelrys.com/products/discovery-studio/>). MD simulations of the solvated models were performed in the NPT ensemble using the NAMD² with the CHARMM22 force-field^{3,4} with CMAP correction.⁵⁻⁹ MD simulations using force-field have demonstrated the sensitivity of the results to details of the backbone potential. The CMAP backbone potential allows some many-body affects to be included in the additive force-field.¹⁰ The grid-based correction CMAP for dihedral angles yields significant improvements in the residue-location specific distribution of the dihedral angle in proteins. The models were energy minimized and explicitly solvated in a TIP3P water box^{11,12} with a minimum distance of 15 Å from each edge of the box. Each water molecule within 2.5 Å of the models was removed. Counter ions were added at random locations to neutralize the models' charge. The Langevin piston method^{2,13,14} with a decay period of 100 fs and a damping time of 50 fs was used to maintain a constant pressure of 1 atm. A temperature of 330 K was controlled by a Langevin thermostat with a damping coefficient of 10 ps⁻¹². The short-range van der Waals interactions were calculated using the switching function, with a twin range cut-off of

10.0 and 12.0 Å. Long-range electrostatic interactions were calculated using the particle mesh Ewald method with a cutoff of 12.0 Å^{15,16}. The equations of motion were integrated using the leapfrog integrator with a step of 1 fs. The solvated systems were energy minimized for 2000 conjugated gradient steps, where the hydrogen bonding distance between the β -sheets in each oligomer was fixed in the range 2.2-2.5 Å. The counter ions and water molecules were allowed to move. The hydrogen atoms were constrained to the equilibrium bond using the SHAKE algorithm¹⁷. The minimized solvated systems were energy minimized for 5000 additional conjugate gradient steps and 20,000 heating steps at 250 K, with all atoms being allowed to move. Then, the system was heated from 250 to 300 K for 300 ps and then equilibrated at 330 K for 300 ps. All simulations were run for 50 ns at 330 K. We ran simulations at a higher temperature than physiological temperature (310 K), in aim to investigate the stability of the constructed models. Obviously, structures that are stable at 330 K will be also stable at lower temperatures. To examine whether the timescale of 50 ns of simulations is a reasonable timescale, we examined the root-mean square deviations (RMSDs) of all constructed models along the time of the simulations. Therefore, these conditions (50 ns and 330K) were applied to all of the examined structures. For the complex kinetics of amyloid formation, this group is likely to represent only a very small percentage of the ensemble. Nevertheless, the carefully selected models cover the most likely organizations.

3. Analysis details

We examined the structural stability of the studied models by following the changes in the number of the hydrogen bonds between β -strands, with the hydrogen bond cut-off being set to 2.5 Å. This examination was performed by following the root-mean square deviations (RMSDs), root-mean square fluctuations (RMSFs) and by monitoring the change in the inter-sheet distance ($C\alpha$ backbone-backbone distance) in the core domain of all of the examined structures. In all the models that we constructed, the core domain of the fibril-like Amylin that were based on models M1, D1 and E1 and M2, D2 and E2 was defined as the distance between residue L12 and residue T30, and that for fibril-like Amylin that are based on M3, D3 and E3 and M4, D4 and E4 as the distance between residue L12 and residue S29. We further investigated the average number of water

molecules around each side-chain C β carbon within 4 Å for the Amylin models. The angles ψ and ϕ of each residue in the Amylin models had been computed for the last 5 ns to estimate the secondary structure of the self-assembled models.

4. Generalized Born method with molecular volume (GBMV)

To obtain the relative conformational energies of the fibril-like structures of all models, the models' trajectories of the last 5 ns were first extracted from the explicit MD simulation excluding the water molecules. The solvation energies of all systems were calculated using the GBMV.^{18,19} In the GBMV calculations, the dielectric constant of water was set to 80. The hydrophobic solvent-accessible surface area (SASA) term factor was set to 0.00592 kcal/ (mol Å²). Each conformer was minimized using 1000 cycles, and the conformational energy was evaluated by grid-based GBMV.

For each set of models (M1-M4, D1-D4 and E1-E4) we estimated the conformational energies as follows. A total of 2000 conformations (500 conformations for each of the 4 examined conformers) were used to construct the energy landscape of the Amylin models and to evaluate the conformer probabilities by using Monte Carlo (MC) simulations. In the first step, one conformation of conformer *i* and one conformation of conformer *j* were randomly selected. Then, the Boltzmann factor was computed as $e^{-(E_j - E_i)/KT}$, where E_i and E_j are the conformational energies evaluated using the GBMV calculations for conformations *i* and *j*, respectively, *K* is the Boltzmann constant and *T* is the absolute temperature (298 K used here). If the value of the Boltzmann factor was larger than the random number, then the transition from conformation *i* to conformation *j* was allowed. After 1 million steps, the conformations that were 'visited' for each conformer were counted. Finally, the relative probability of conformer *n* was evaluated as $P_n = N_n/N_{total}$, where P_n is the population of conformer *n*, N_n is the total number of conformations visited for the conformer *n*, and N_{total} is the total steps. The advantages of using MC simulations to estimate conformer probability lie in their good numerical stability and the control that they allow of the transition probabilities among several conformers.

Using all 4 conformers and 2000 conformations (500 for each conformer) generated from the MD simulations, we estimated the overall stability and populations for each conformer based on the MD simulations, with the energy landscape being computed with

GBMV for all conformers. It should be noted here, that we compared the relative conformational energies (and not free energies) between the models. For the complex kinetics of amyloid formation, the group of the 4 conformers is likely to represent only a very small percentage of the ensemble. Nevertheless, the carefully selected models cover the most likely structures.

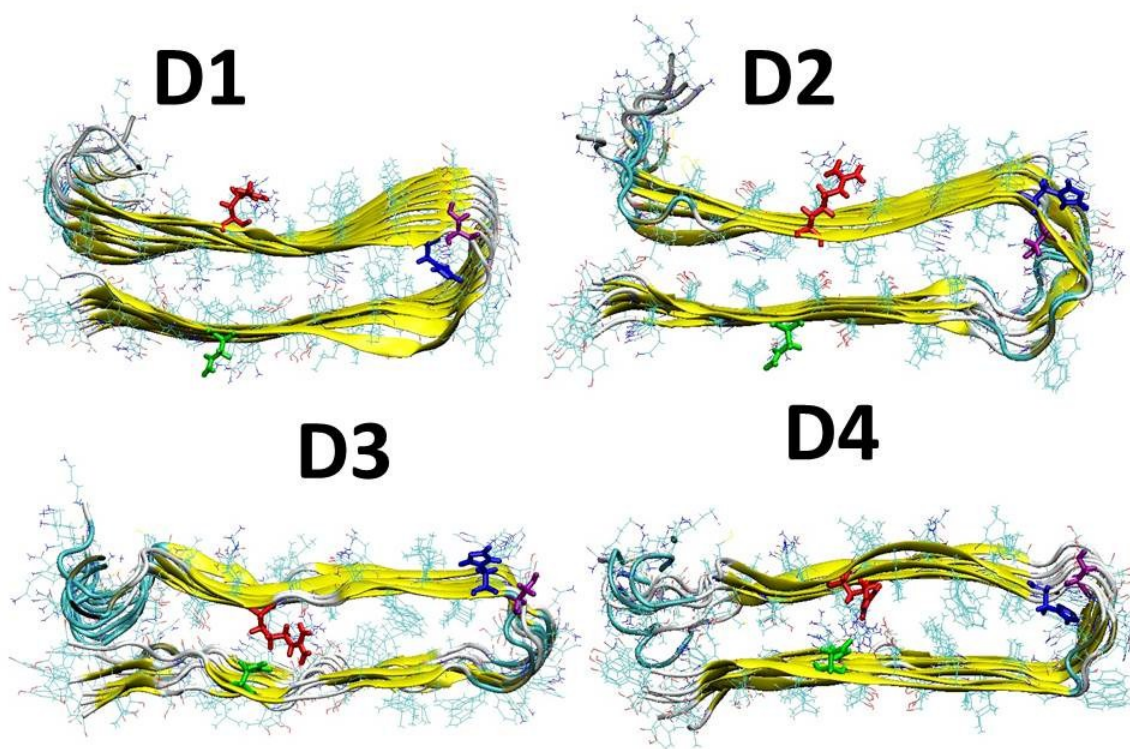


Figure S1: Initial constructed models D1-D4 of amylin oligomers, after removal of the disulfide bonds Cys2-Cys7 in models M1-M4 (models M1-M4 were taken from our previous study¹).

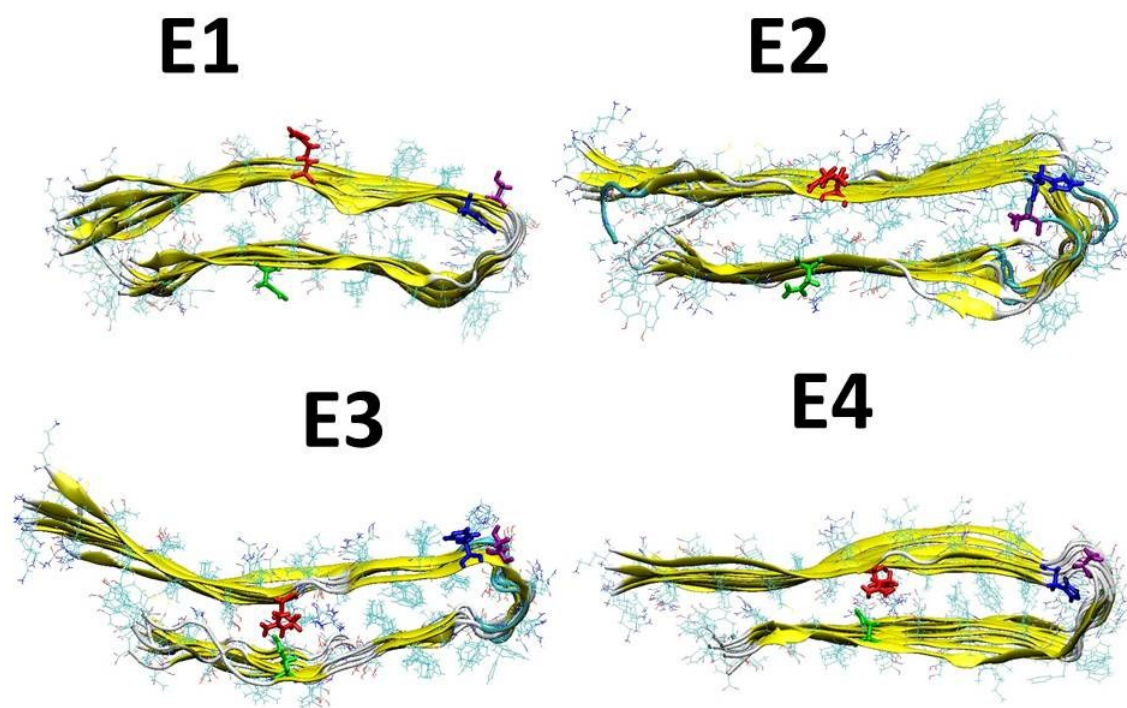


Figure S2: Initial constructed models E1-E4 of amylin oligomers, after removal of the disulfide bonds Cys2-Cys7 in models M1-M4 (models M1-M4 were taken from our previous study¹).

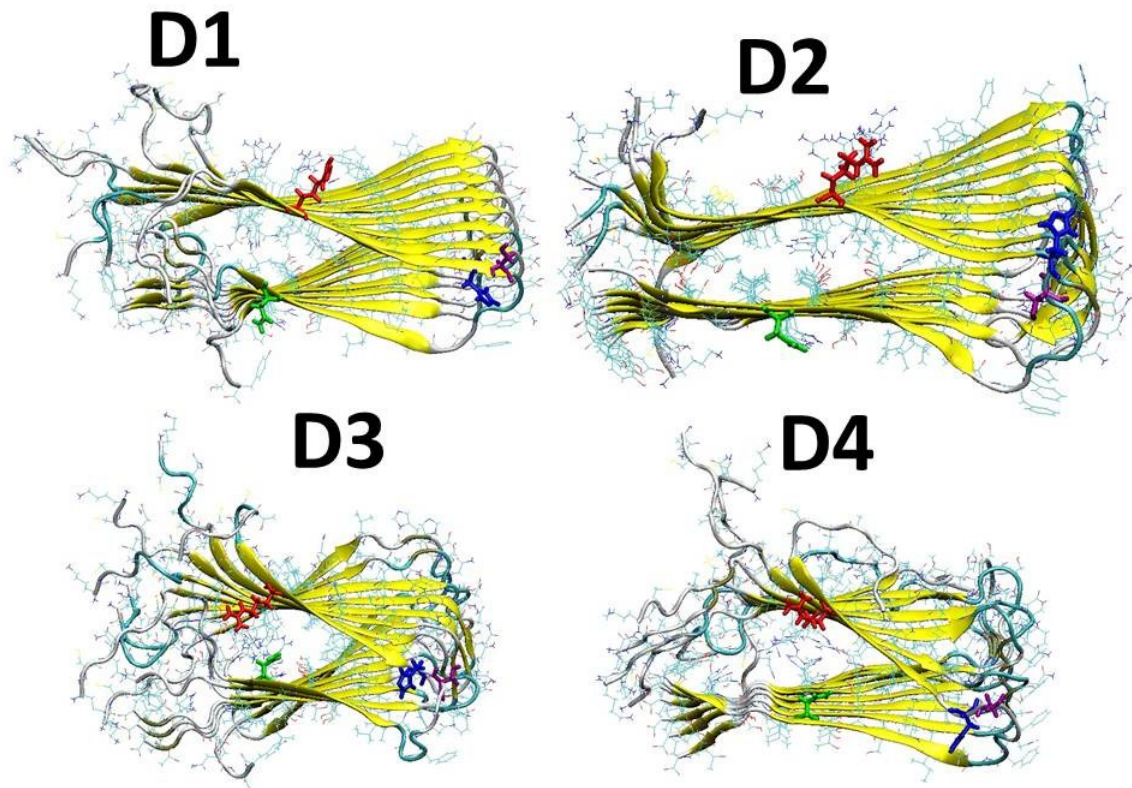


Figure S3: Simulated models D1-D4 of amylin oligomers, after removal of the disulfide bonds Cys2-Cys7 in models M1-M4 (models M1-M4 were taken from our previous study¹).

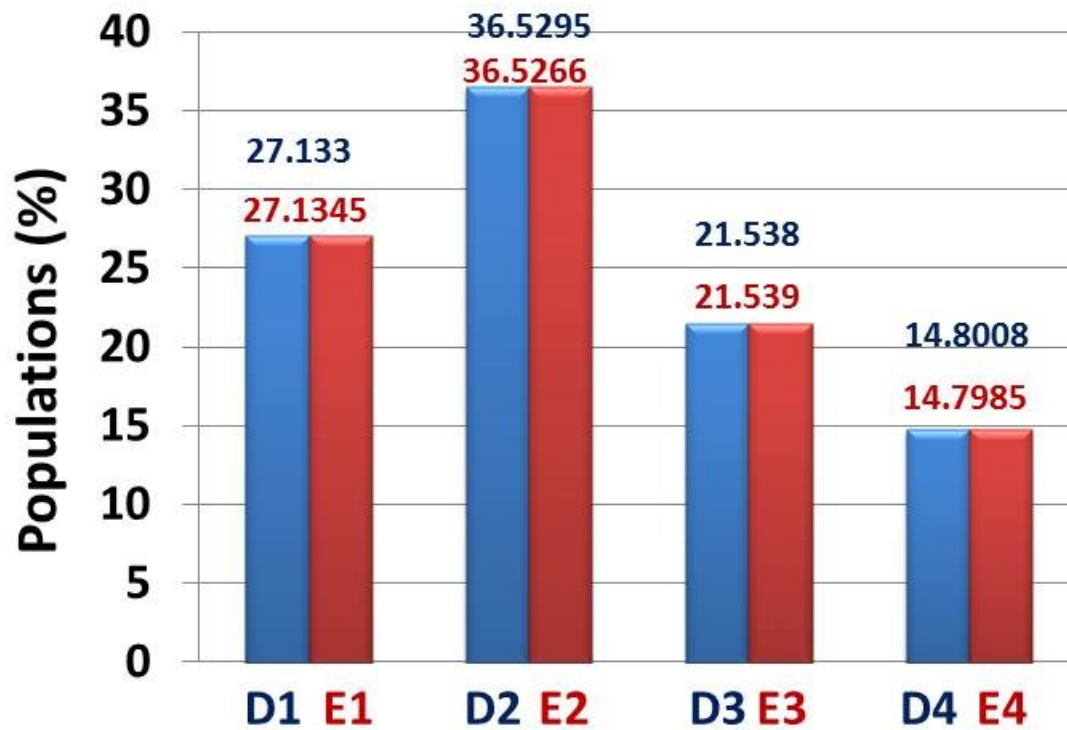


Figure S4: Populations of the simulated models D1-D4 and E1-E4 of amylin oligomers using Monte Carlo simulations.

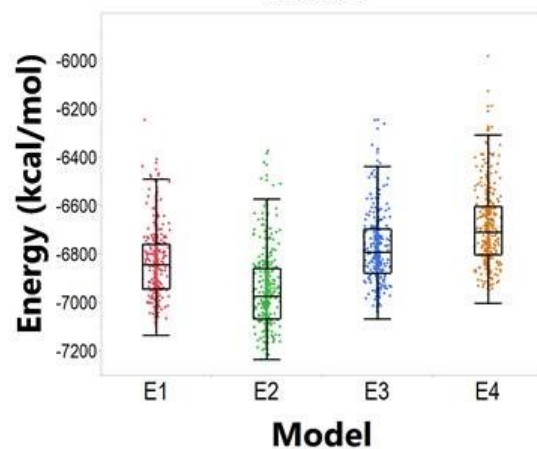
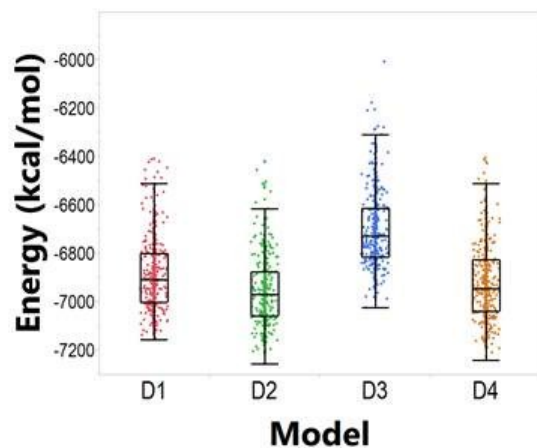
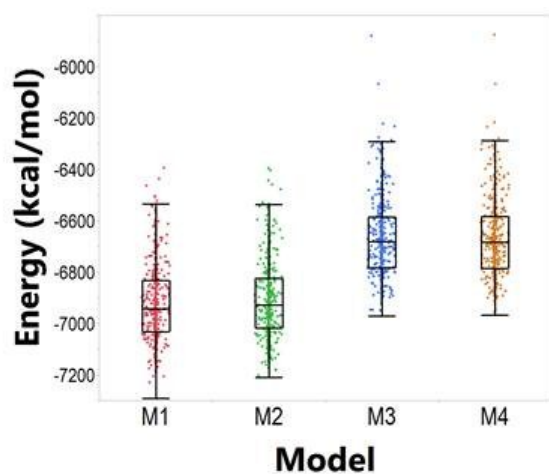


Figure S5: Distributions of the conformational energy values of the simulated models M1-M4, D1-D4 and E1-E4 of amylin oligomers obtained from the GBMV calculations.^{20,21}

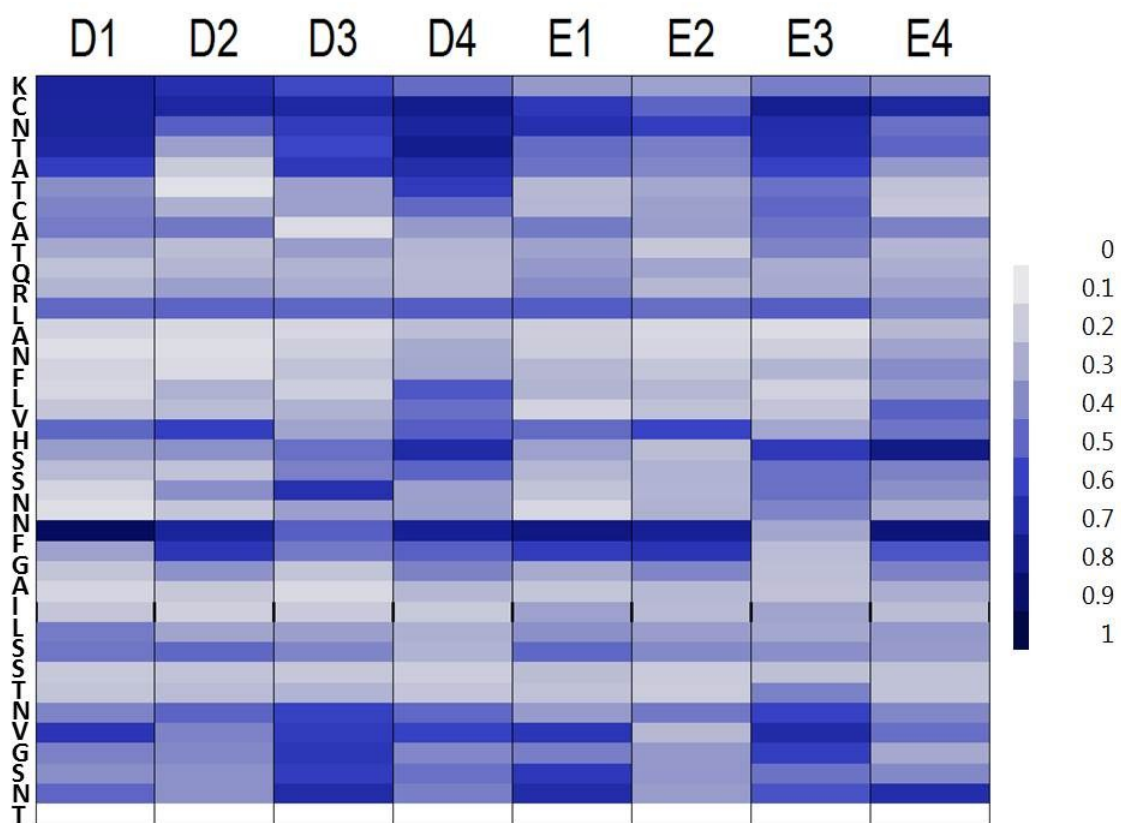


Figure S6: The average number of water molecules around each side chain C β carbon (within 4 Å) for the simulated models D1-D4 and E1-E4.

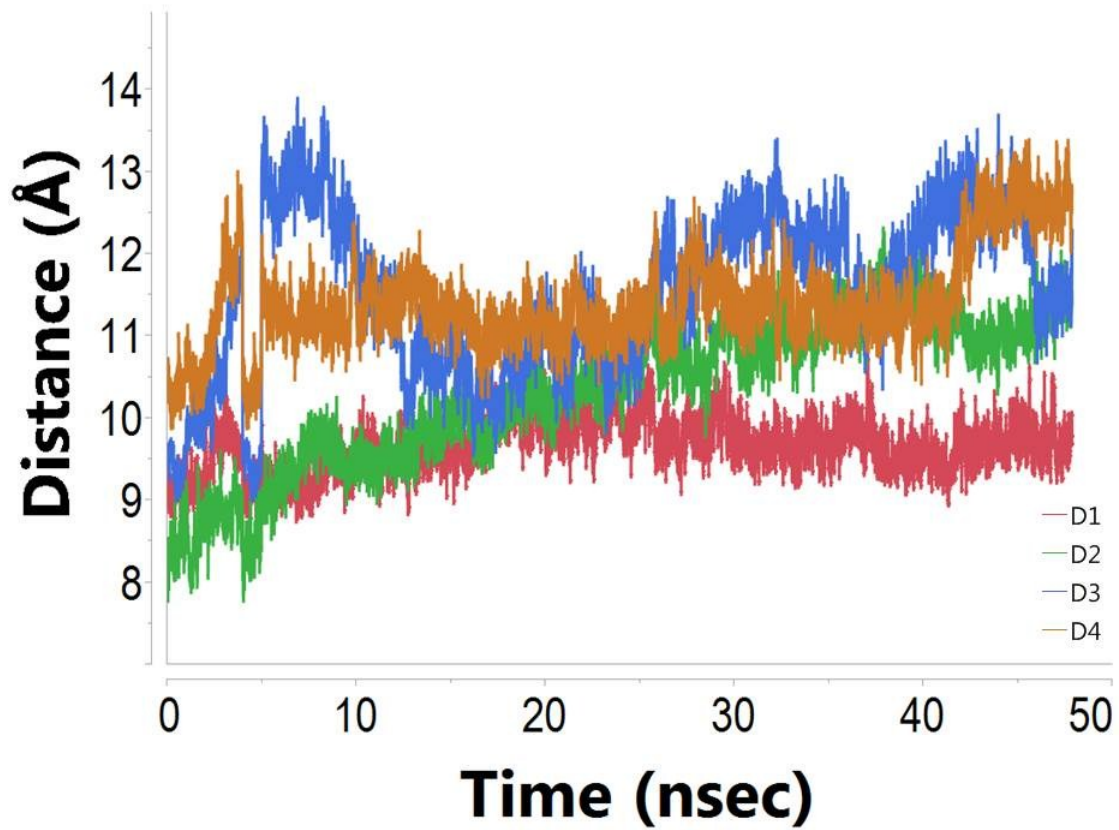


Figure S7: The averaged inter-sheet ($C\alpha$ backbone-backbone) distances for models D1-D4 along the molecular dynamics (MD) simulations.

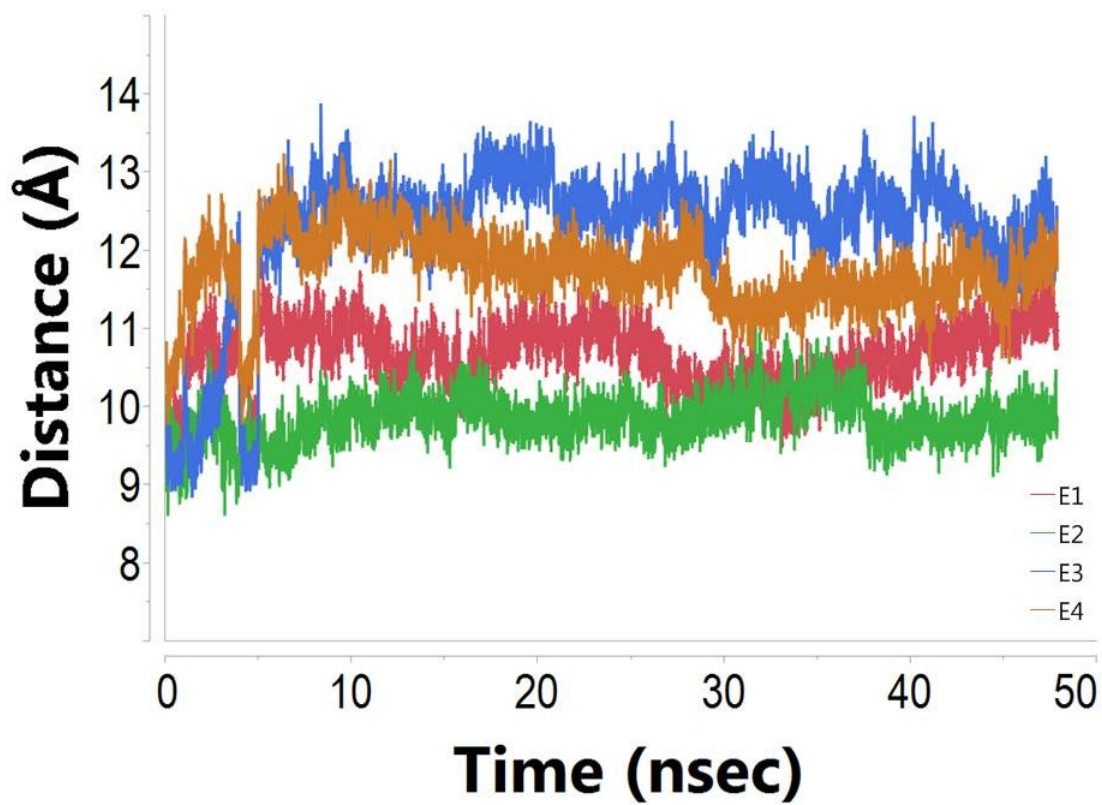


Figure S8: The averaged inter-sheet ($C\alpha$ backbone-backbone) distances for models E1-E4 along the molecular dynamics (MD) simulations.

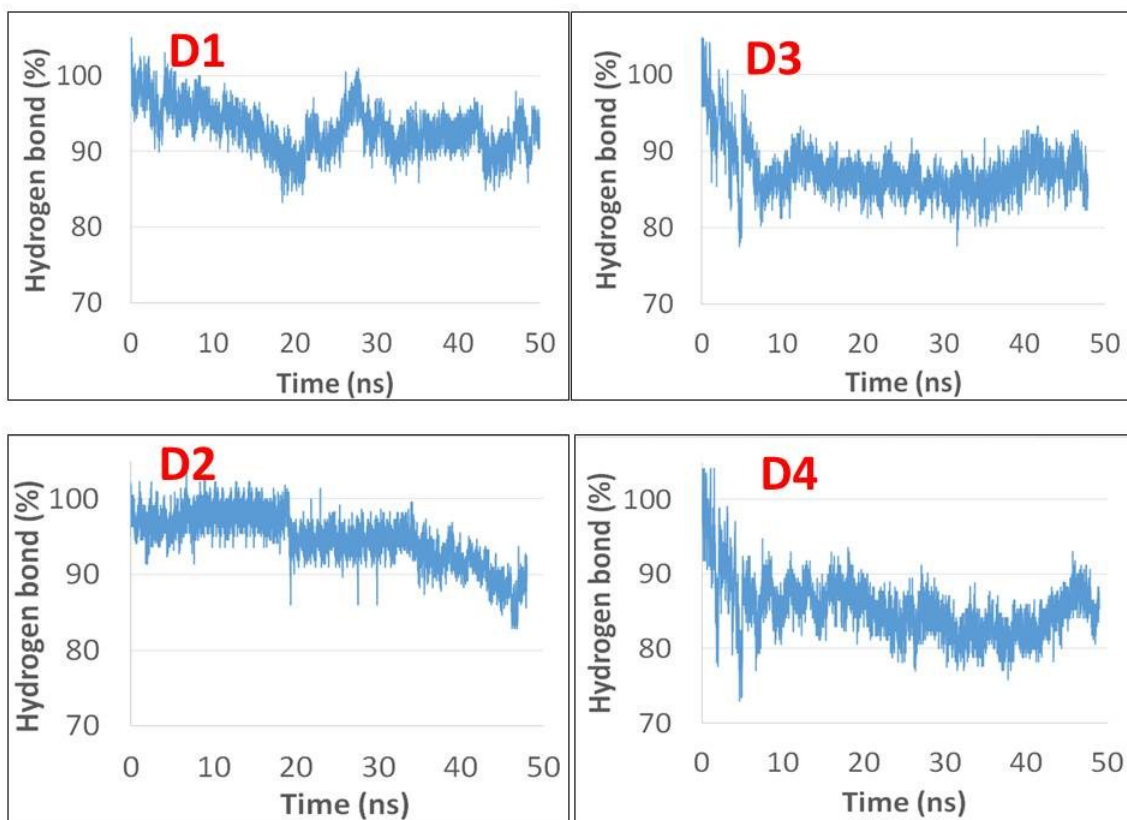


Figure S9: The fraction of the number of hydrogen bonds (in percentage) between all β -strands compare to the number in the initial constructed model, for models D1-D4.

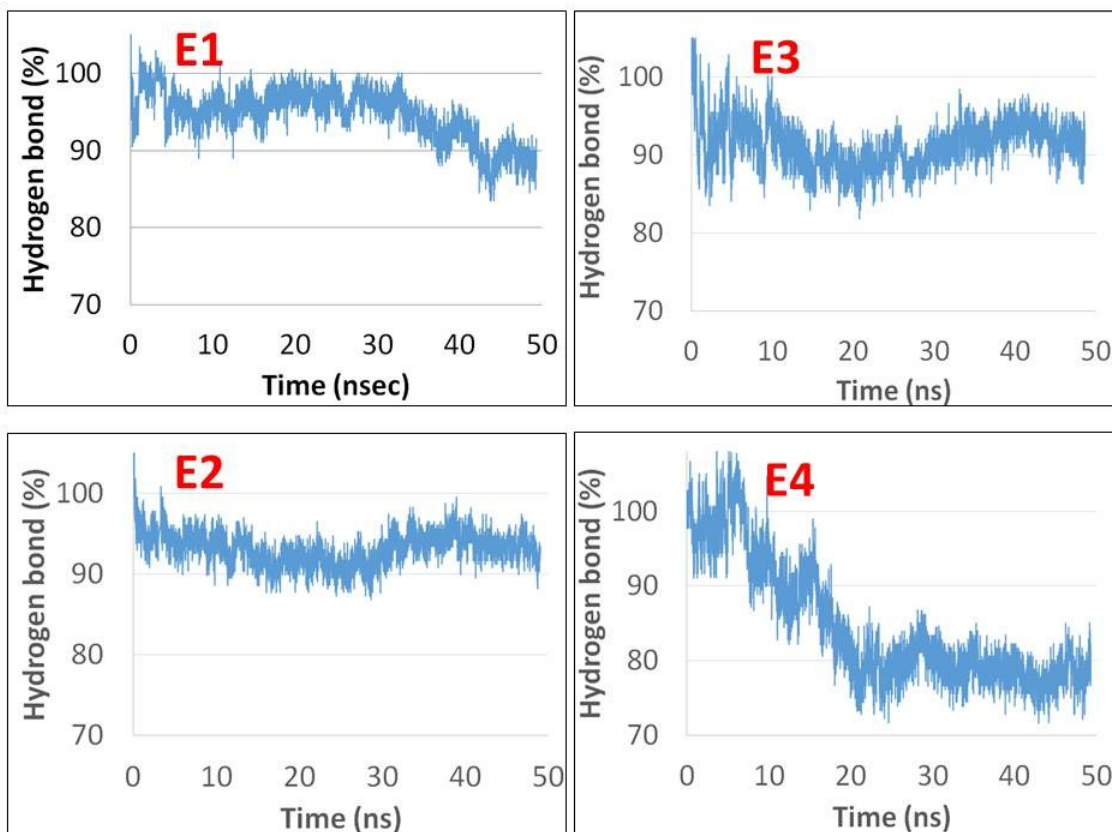


Figure S10: The fraction of the number of hydrogen bonds (in percentage) between all β -strands compare to the number in the initial constructed model, for models E1-E4.

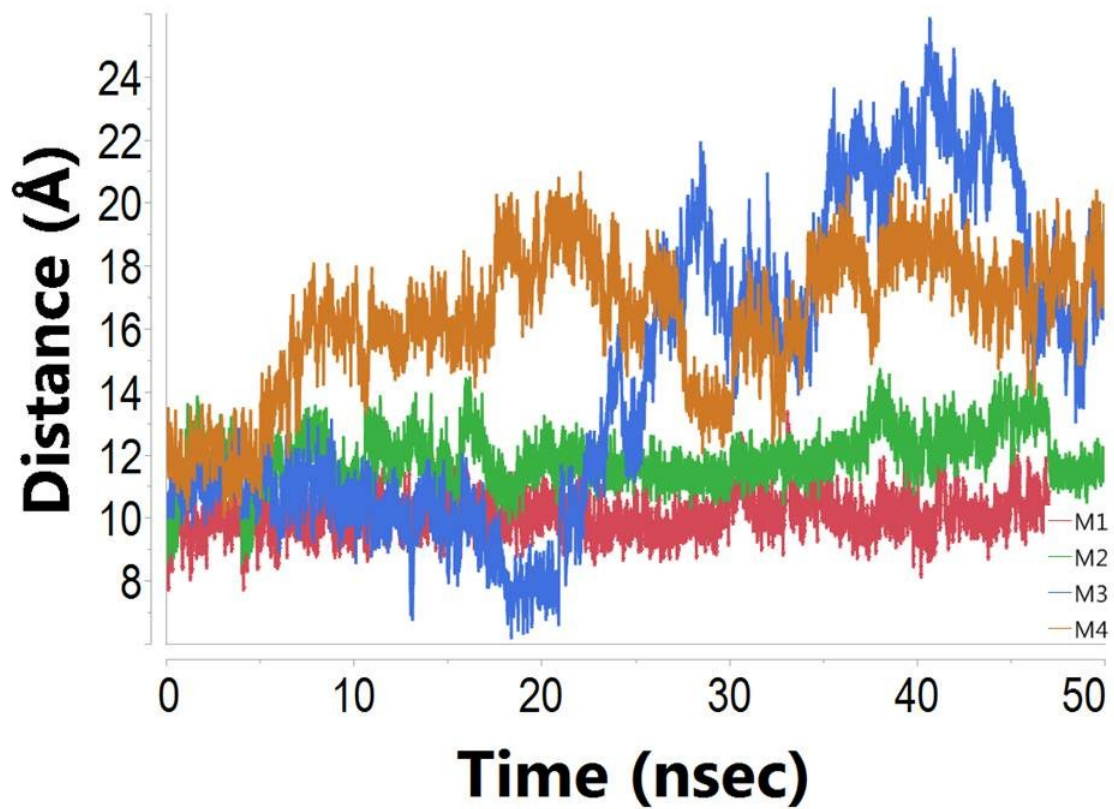


Figure S11: The averaged inter-sheet ($C\alpha$ backbone-backbone) distances for models M1-M4 along the molecular dynamics (MD) simulations.

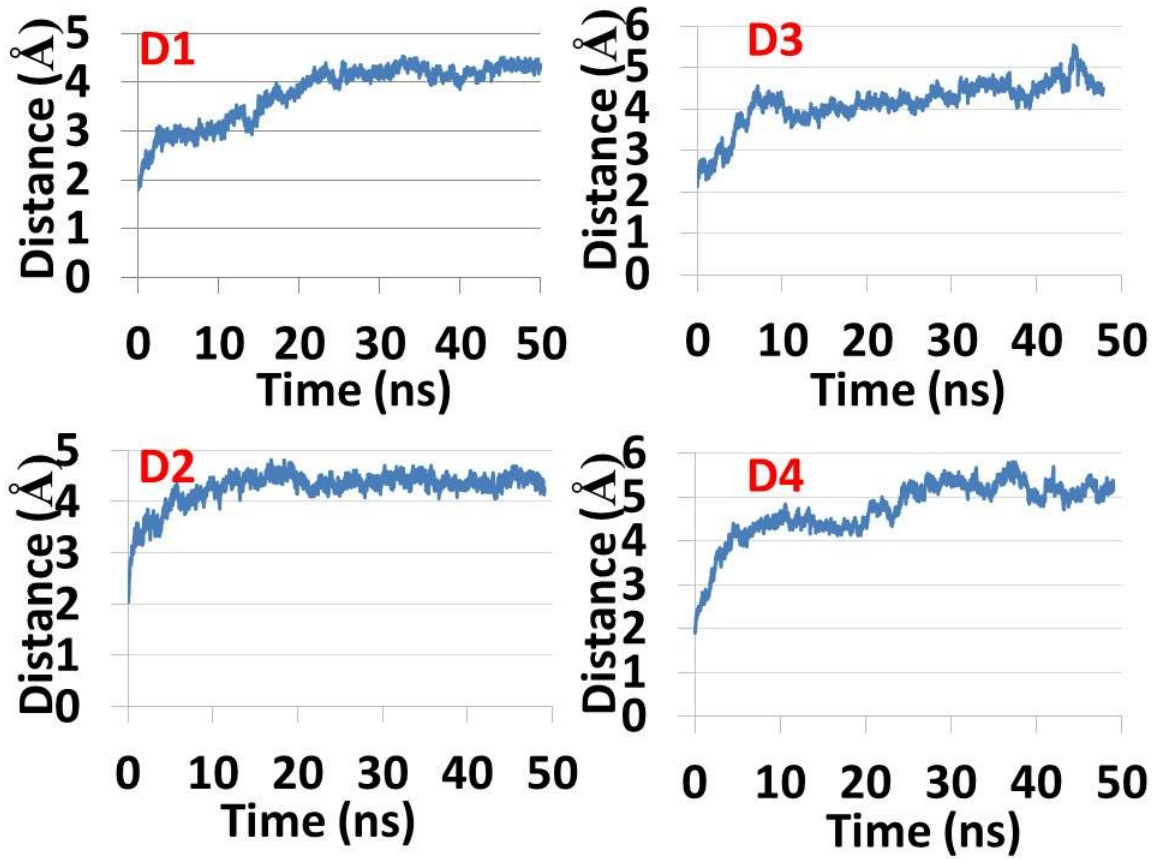


Figure S12: RMSDs of models D1-D4.

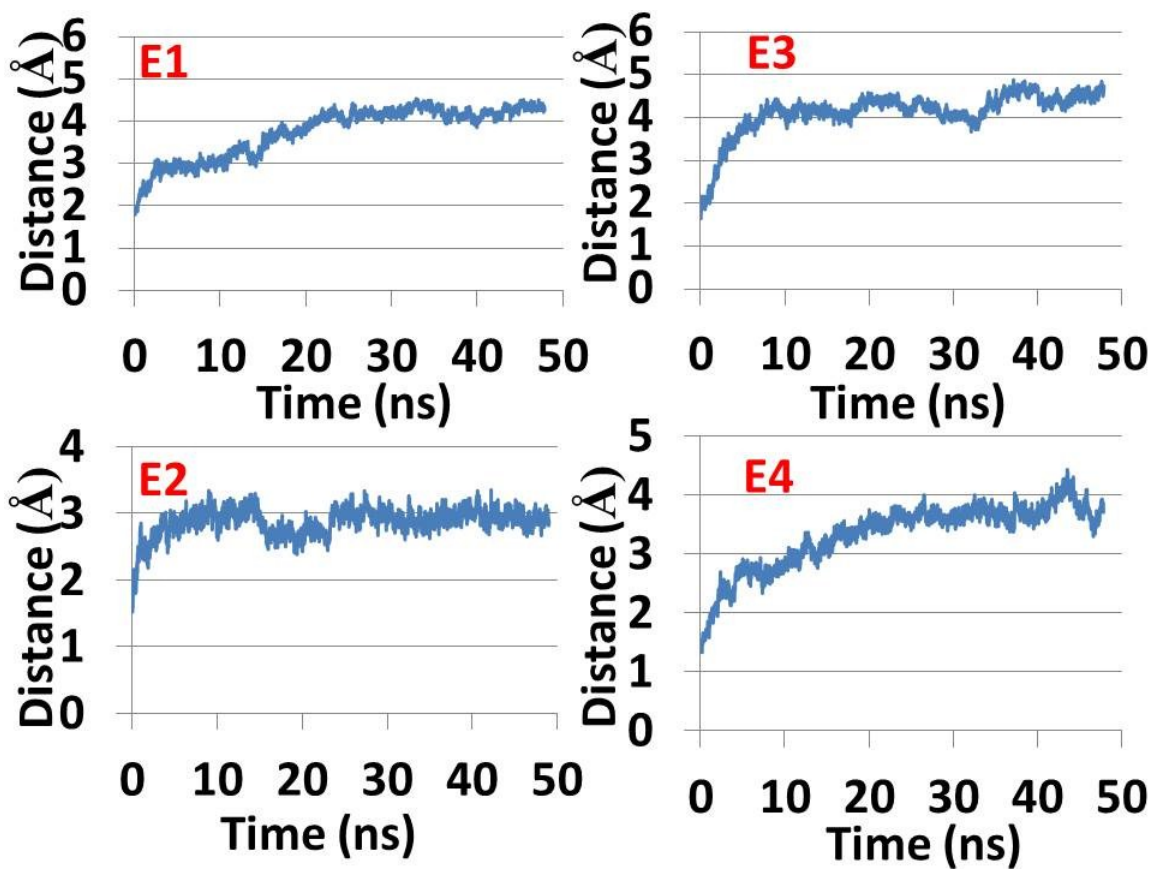


Figure S13: RMSDs of models E1-E4.

Table S1: The conformational energies (computed using the GBMV^{22,23} calculations) and the populations of the studied models. Standard deviations are in parenthesis.

Model	Energy (kcal/mol)	Populations (%)
M1	-6921(149)	34.97
M2	-6908(147)	34.10
M5	-6668(151)	15.44
M6	-6668(151)	15.47
D1	-6892(149)	27.13
D2	-6959(139)	36.52
D3	-6704(156)	21.53
D4	-6925(159)	14.80
E1	-6841(143)	27.13
E2	-6956(156)	36.52
E3	-6776(143)	21.54
E4	-6690(157)	14.79

Table S2: The helicity pitch values of all models of amylin oligomers of the studied models. The experimental helicity pitch value is 240Å.²⁴

	Helicity pitch (Å)
M1	201 (18)
M2	274 (4.5)
M3	246 (5)
M4	166 (4.3)
D1	267 (27)
D2	684 (172)
D3	299 (19)
D4	408 (82)
E1	360 (4)
E2	359 (54)
E3	265 (30)
E4	231 (22)

References:

- (1) Wineman-Fisher, V.; Atsmon-Raz, Y.; Miller, Y. *Biomacromolecules* **2015**, *16*, 156.
- (2) Kalé, L.; Skeel, R.; Bhandarkar, M.; Brunner, R.; Gursoy, A.; Krawetz, N.; Phillips, J.; Shinozaki, A.; Varadarajan, K.; Schulten, K. *Journal of Computational Physics* **1999**, *151*, 283.
- (3) MacKerell, A. D.; Bashford, D.; Bellott, R. L.; Dunbrack, R. L.; Evanseck, J. D.; Field, M. J.; Fischer, S.; Gao, J.; Guo, H.; Ha, S.; Joseph-McCarthy, D.; Kuchnir, L.; Kuczera, K.; Lau, F. T. K.; Mattos, C.; Michnick, S.; Ngo, T.; Nguyen, D. T.; Prodhom, B.; Reiher, W. E.; Roux, B.; Schlenkrich, M.; Smith, J. C.; Stote, R.; Straub, J.; Watanabe, M.; Wiórkiewicz-Kuczera, J.; Yin, D.; Karplus, M. *Journal of Physical Chemistry B (Formerly : Journal of Physical Chemistry 1952)* **1998**, *102*, 3586.
- (4) Brooks, B. R.; Bruccoleri, R. E.; Olafson, B. D.; States, D. J.; Swaminathan, S.; Karplus, M. *Journal of Computational Chemistry* **1983**, *4*, 187.
- (5) Cino, E. A.; Choy, W. Y.; Karttunen, M. *J Chem Theory Comput* **2012**, *8*, 2725.
- (6) Mackerell, A. D., Jr.; Feig, M.; Brooks, C. L., 3rd *Journal of computational chemistry* **2004**, *25*, 1400.
- (7) Best, R. B.; Buchete, N. V.; Hummer, G. *Biophys J* **2008**, *95*, L07.
- (8) Freddolino, P. L.; Park, S.; Roux, B.; Schulten, K. *Biophys J* **2009**, *96*, 3772.
- (9) Lindorff-Larsen, K.; Maragakis, P.; Piana, S.; Eastwood, M. P.; Dror, R. O.; Shaw, D. E. *PLoS One* **2012**, *7*, e32131.
- (10) Best, R. B.; Mittal, J.; Feig, M.; MacKerell, A. D., Jr. *Biophys J* **2012**, *103*, 1045.
- (11) Mahoney, M. W.; Jorgensen, W. L. *The Journal of Chemical Physics* **2000**, *112*, 8910.
- (12) Jorgensen, W. L.; Chandrasekhar, J.; Madura, J. D.; Impey, R. W.; Klein, M. L. *The Journal of Chemical Physics* **1983**, *79*, 926.
- (13) Tu, K.; Tobias, D. J.; Klein, M. L. *Biophysical journal* **1995**, *69*, 2558.
- (14) Feller, S. E.; Zhang, Y.; Pastor, R. W.; Brooks, B. R. *The Journal of Chemical Physics* **1995**, *103*, 4613.
- (15) Essmann, U.; Perera, L.; Berkowitz, M. L.; Darden, T.; Lee, H.; Pedersen, L. G. *The Journal of Chemical Physics* **1995**, *103*, 8577.

- (16) Darden, T.; York, D.; Pedersen, L. *The Journal of Chemical Physics* **1993**, *98*, 10089.
- (17) Ryckaert, J.-P.; Ciccotti, G.; Berendsen, H. J. C. *Journal of Computational Physics* **1977**, *23*, 327.
- (18) Lee, M. S.; Feig, M.; Salsbury, F. R., Jr.; Brooks, C. L., 3rd *Journal of computational chemistry* **2003**, *24*, 1348.
- (19) Lee, M. S.; Salsbury, J. F. R.; Brooks III, C. L. *The Journal of Chemical Physics* **2002**, *116*, 10606.
- (20) Lee, M. S.; Feig, M.; Salsbury, F. R.; Brooks, C. L. *J Comput Chem* **2003**, *24*, 1348.
- (21) Lee, M. S.; Salsbury, F. R.; Brooks, C. L. *J Chem Phys* **2002**, *116*, 10606.
- (22) Lee, M. S.; Feig, M.; Salsbury, F. R.; Brooks, C. L. *Journal of Computational Chemistry* **2003**, *24*, 1348.
- (23) Lee, M. S.; Salsbury, F. R.; Brooks, C. L. *J Chem Phys* **2002**, *116*, 10606.
- (24) Bedrood, S.; Li, Y.; Isas, J. M.; Hegde, B. G.; Baxa, U.; Haworth, I. S.; Langen, R. *The Journal of biological chemistry* **2012**, *287*, 5235.